

Effects of Electron Irradiation on Methylthiolate Monolayer on Au(111): Electron-Stimulated Desorption

H. Kondoh and H. Nozoye*

National Institute of Materials and Chemical Research, Tsukuba, Ibaraki 305-8565, Japan

Received: July 3, 1997; In Final Form: January 13, 1998

Effects of electron irradiation on a methylthiolate (CH_3S) self-assembled monolayer on Au(111) have been studied by using scanning tunneling microscope (STM), Auger electron spectroscopy (AES), low-energy electron diffraction, and thermal-desorption spectroscopy (TDS). AES results indicated that irradiation of the $\text{CH}_3\text{S}/\text{Au}(111)$ surface by an electron beam induces electron-stimulated desorption (ESD), in which mainly the methyl moiety desorbs via S–C bond cleavage, leaving a sulfur atom on the surface. From a quantitative analysis of TD spectra, the cross section of the ESD is estimated to be $2.8 \times 10^{-17} \text{ cm}^2$ for 100-eV electrons. Two-dimensional arrangements of the methylthiolate and the sulfur species under the ESD process have been investigated with STM. The STM observations indicated that the sulfur adatoms form 2D islands that grow in size with the progress of the ESD process, while unaffected methylthiolates are distributed between the sulfur islands. After the completion of the ESD, the Au(111) surface is covered with small patches ($\lesssim 100 \text{ \AA}$) of sulfur domains.

Introduction

Self-assembly of sulfur-containing organic molecules such as alkanethiols or dialkyl disulfides on metal and semiconductor surfaces is an easy and convenient method for preparing highly ordered organic monolayers.¹ These monolayers have received considerable attention not only because they are important to the fundamental understanding of the self-assembly phenomena² but also because they have potential use in technological applications such as corrosion inhibition, tribology, molecular recognition, biosensors, and nanofabrication.³

In developing new functional materials using these types of organic monolayers, the ability to pattern the monolayers with micrometer or nanometer spatial resolution is one of the crucial points. So far, effective methods for patterning of organothiol monolayers have been extensively explored by using various techniques such as mechanical scratching,⁴ UV photopatterning,^{5–9} microlithography using electron beam,^{10–13} ion beam,¹³ and neutral-atom beam,¹⁴ scanning tunneling microscope (STM)-tip-induced lithography,^{15–17} and microcontact printing with elastomeric stamps.^{18,19} The smallest patterned sizes using these techniques reach levels of 60 nm for the electron-beam lithography¹² and 10 nm for the STM lithography,¹⁵ which are comparable to the scale of an array of several tens of thiol molecules. The smaller the patterned size is, the more desirable the molecular-level understanding of the structures in the patterned area is. However, the structures in the patterned area have been scarcely investigated on a molecular level; only one STM study after STM-tip lithography has been reported.¹⁵

In most cases of beam-irradiation lithography, it is a common phenomenon that some decomposition of the molecules occurs in the beam-irradiated areas. Residual species after such decomposition must have effects on subsequent procedures. These procedures include refilling of another type of species in the irradiated areas and further etching of the irradiated areas.

Therefore, it is quite important to understand what occurs in the irradiated areas and what structure is formed there. Nevertheless, only X-ray beam damage has been studied by Whitesides et al. for CF_3 -terminated thiol monolayers on metal surfaces, and they concluded that not X-ray photons themselves but X-ray-generated primary and secondary electrons are the principal causes of removal of the fluorine from the monolayers.^{20,21} However, it is still unclear what kinds of effects other than the loss of the terminal fluorine are given to the monolayers upon irradiation. Furthermore, no study has so far addressed structural changes of thiol monolayers after beam irradiation.

In this work, we have investigated effects of electron-beam irradiation on methylthiolate (CH_3S) monolayer on Au(111), which is the simplest system of this kind, by using combined surface techniques of Auger electron spectroscopy (AES), low-energy electron diffraction (LEED), thermal-desorption spectroscopy (TDS), and STM. The electron irradiation mainly gives rise to electron-stimulated desorption (ESD) of the methyl moiety via S–C bond breaking, which leaves sulfur atoms on the surface. We will also report here mesoscopic- and microscopic-scale changes of the structure of the methylthiolate/Au(111) interface during the ESD process. Electron-induced sulfur species and unaffected methylthiolates exhibit specific mesoscopic structures via significant surface diffusion.

Experimental Section

The experiments were performed with an ultrahigh-vacuum (UHV) STM system (JEOL, JSTM-4500XT), which is equipped with facilities for AES, LEED, and TDS. Au(111) single-crystal thin films were prepared using the vacuum deposition method on cleaved mica at a substrate temperature of 350 °C. The Au(111) surface was cleaned by Ar-ion sputtering and was annealed under UHV conditions. The cleanliness and ordering were confirmed by AES, LEED, and STM. The $23 \times \sqrt{3}$ reconstruction, which is specific to clean Au(111), was clearly observed by STM. The Au(111) surfaces were exposed to gaseous dimethyl disulfide (CH_3SSCH_3) at room temperature,

* Corresponding author. E-mail: nozoye@nimc.go.jp. Fax: +81 298 54 4504.

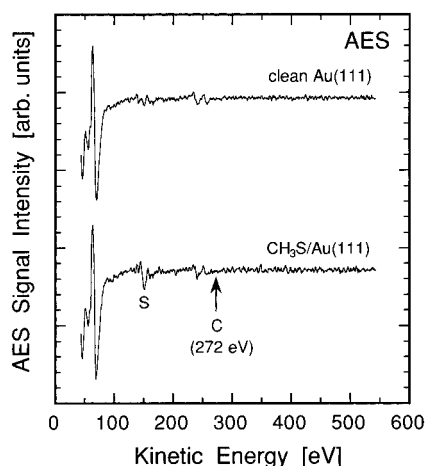


Figure 1. AES spectra for a clean Au(111) surface (upper) and a methylthiolate-covered Au(111) surface (lower). For preparing the methylthiolate/Au(111) surface, a clean Au(111) surface was exposed to 17 langmuirs of gaseous dimethyl disulfide at room temperature. A primary electron-beam energy of 4 keV was used for the AES measurements.

which was introduced into the vacuum chamber via a variable-leak valve. Dimethyl disulfide is known to dissociate spontaneously on Au(111) into methylthiolates at room temperature.²² AES and TDS measurements have revealed that a saturated layer was formed by exposing the vapor to more than 2 langmuirs (1 langmuir = 10^{-6} Torr s) at room temperature.

AES and LEED electron guns were operated with typical electron-beam fluxes of 1×10^{16} [electrons $\text{cm}^{-2} \text{s}^{-1}$] at 4 keV and 2.5×10^{15} [electrons $\text{cm}^{-2} \text{s}^{-1}$] at 100 eV. TDS measurements were performed with a mass spectrometer at a heating rate of 9 K/s. STM measurements were carried out under UHV conditions at room temperature under constant-current mode by using an electrochemically prepared tungsten tip. Tunneling conditions used here were typically bias voltages ranging from 1 to 2 V and tunneling currents of around 50 pA unless otherwise stated. All STM images were processed with a mild low-pass filter to remove high-frequency noises.

Results and Discussion

A. Evidence for ESD Provided from LEED, AES, and TDS. First, we checked long-range ordering of the methylthiolate monolayer on Au(111) by LEED. It exhibited a fairly diffuse ($\sqrt{3} \times \sqrt{3}$)R30° LEED pattern. During the LEED observation, the ($\sqrt{3} \times \sqrt{3}$)R30° spots gradually became dim and completely disappeared within 20 s, which was also observed in a previous study.²³ The quick disappearance of the LEED spots suggests that the LEED electron beam (50–300 eV) significantly damages the monolayer, resulting in destruction of the ordering. No other fractional-order spots were clearly observed.

Figure 1 shows AES spectra for a clean Au(111) surface and a saturated monolayer of methylthiolate on Au(111). Although an AES peak due to sulfur species is clearly observed at 150 eV, no feature appears at 272 eV where carbon structures should be observed. The absence of the carbon AES peak indicates that the carbon species is efficiently removed from the surface by electron irradiation during the AES measurements. This means that electron-stimulated decomposition/desorption of the methylthiolate occurs in which the S–C bond is cleaved and the methyl moiety desorbs, leaving a sulfur adatom.

The electron-stimulated decomposition/desorption of methylthiolate was supported by TDS measurements of dimethyl

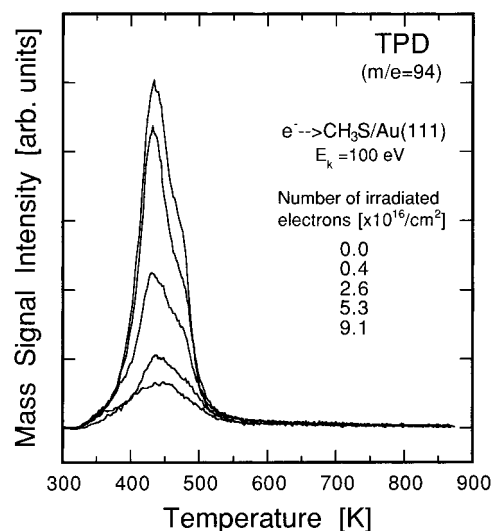


Figure 2. TD spectra for desorption of dimethyl disulfide ($m/e = 94$) from methylthiolate-covered Au(111) surfaces after electron irradiation. The electron irradiation was carried out by careful driving of the sample parallel to the surface with exposure to a fixed electron beam from the LEED electron gun (the electron-beam energy used was 100 eV, the beam current $3.6 \mu\text{A}$, and the beam diameter 1.1 mm) in such a manner that the whole surface was uniformly irradiated. The number of irradiated electrons was varied from 0 to 9.1×10^{16} electrons/ cm^2 .

disulfide. Methylthiolates bound to Au(111) desorb associatively as dimethyl disulfide upon heating.²² TD spectra of dimethyl disulfide are shown in Figure 2 as a function of electron exposure. The whole surface was uniformly exposed to the electron beam from the LEED electron gun by shifting the sample position parallel to the surface. The electron-beam energy used was 100 eV. The TD spectrum without electron irradiation exhibited a desorption peak at 430 K with a shoulder at higher temperature, which is in good agreement with that reported by Nuzzo et al.²² As the electron exposure is increased, the peak intensity is reduced and the peak maximum shifts to higher temperatures, which indicates that the amount of methylthiolate is decreased by electron irradiation. No species other than dimethyl disulfide thermally desorb from the surface after electron irradiation. Considering the fact that the sulfur AES signal remains observable after electron irradiation, the methylthiolate is not desorbed during this ESD process, but the methyl moiety is desorbed, leaving the sulfur atom. In the present case, desorption species during the ESD process could not be directly detected with the mass spectrometer. There is no direct evidence to determine whether the methyl moiety desorbs as methyl radical, methyl cation, ethane, or other species, although desorption of a methyl radical or methyl cation is suggested as described below. It is interesting to note that Yates et al. studied electron-beam-induced surface chemistry for methoxy(CH_3O)/Al(111), which is an analogue to the present system, and found the preferential rupture of C–O bonds.²⁴ Further, cross sections for desorption of neutral methoxy radicals and H^+ ions have been found to be 2 and 5 orders of magnitude, respectively, smaller than that for the C–O bond cleavage.²⁵

The TD peak intensity is plotted as a function of electron exposure in Figure 3. The density of methylthiolate is indicated on the left vertical axis, assuming that the density of the saturated monolayer without electron irradiation is $1/3$ of the Au(111) surface-atom density (1.38×10^{15} atoms/ cm^2) because of the observation of the ($\sqrt{3} \times \sqrt{3}$)R30° LEED pattern. For the other alkylthiolates, the saturated density on Au(111) at room tem-

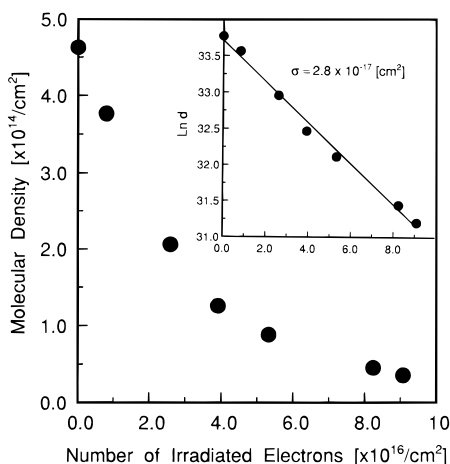


Figure 3. Change of the density of surface methylthiolates (d) as a function of the number of irradiated electrons. Inset: A semilog plot for the change of the methylthiolate density d as a function of the number of irradiated electrons. The solid line shows the result of linear fitting to the data.

perature has been reported to be also $1/3$ by STM and diffraction studies.^{23,26–29} The methylthiolate density decreases in an exponential-like manner with electron exposure, which is more clearly seen on a semilog plot for the density changes shown in the inset; an almost linear decay is observed. From the slope of the linear fit, the cross section of the ESD process is estimated to be $2.8 \times 10^{-17} \text{ cm}^2$. The disappearance of the LEED spots within 20 s stated above can be explained by this cross section because more than 80% of the methylthiolate was decomposed and desorbed in 20 s with our LEED electron gun. The exponential-like decrease of the methylthiolate density indicates that the ESD of methylthiolate obeys first-order kinetics, which suggests that methyl radicals or methyl cations desorb from the surface.

B. STM Observations for the ESD Process. From the combined results of LEED, AES, and TDS, it has been revealed that electron irradiation on the methylthiolate monolayer induces an ESD where the methyl moiety is removed via S–C bond cleavage, resulting in the sulfur atom remaining on the surface. To understand how the sulfur species and unaffected methylthiolate species behave on the Au(111) surface, we observed STM images for a series of methylthiolate/Au(111) surfaces after a series of electron exposures. Since the sample was transferred from an STM-measurement position when it was exposed to the electron beam, imaged areas were different after each exposure.

Figure 4a shows an STM image of a saturated monolayer of methylthiolate taken at room temperature without electron irradiation. The brighter area in the top-right region is an upper terrace with monatomic height, since the height difference between the upper and lower terraces is 2.3 Å, which is in agreement with the monatomic height of Au(111) (2.35 Å). No feature associated with molecular arrangements are observed, even though it was confirmed by AES and TDS that the surface is covered with a full monolayer of methylthiolate. This is probably due to fast motion of the methylthiolate (diffusion or fluctuation of conformation) compared with the scan rate of the STM tip ($\sim 20 \text{ Å/ms}$). In fact, 2D molecular arrangements were certainly observed when STM images were taken at low temperature (90 K) for the same sample.³⁰ The motion of the methylthiolate could be suppressed at low temperature. Although the molecular image is invisible at room temperature for methylthiolate adsorbed on Au(111), it is indeed visible for

thiolates with the longer alkyl chain ($\text{CH}_3(\text{CH}_2)_n\text{S}$; $n \geq 1$) on Au(111) even at room temperature.^{2,26–28,31} Thus, the fast motion of methylthiolate might originate from a relatively weak methyl–methyl intermolecular interaction.

In Figure 4b is shown an STM image for a surface after a low dose of electrons ($1.6 \times 10^{15} \text{ electrons/cm}^2$). Dark spots with a diameter of ca. 10 Å randomly appear over the surface. Since the apparent depth of the dark spots is only 0.6 Å, they cannot be attributed to monatomic-height Au vacancies but to defects of methylthiolate monolayer induced by electron irradiation. An increase of the dose of electrons ($7.8 \times 10^{15} \text{ electrons/cm}^2$) gives rise to an increase in the average area of the dark regions by a factor of ca. 5 as shown in Figure 4c. It should be noted that the dark regions have a rectangular-like shape and their long axes are parallel to the three equivalent $\langle 1\bar{2}1 \rangle$ directions, which are rotated by 30° from the Au close-packed rows. A detailed description of this characteristic structure will be given below. A further increase of the dose of electrons ($3.9 \times 10^{16} \text{ electrons/cm}^2$) causes growth of the size of the dark regions, and their shapes become irregular as shown in Figure 4d. In contrast, the fraction of bright regions is significantly reduced, less than 20% of the whole surface. From this series of STM images, we conclude that the dark regions, which grow in size with electron exposure, are 2D islands of the sulfur species formed by ESD from methylthiolate, while the bright regions are ascribed to unaffected methylthiolates. The unaffected methylthiolates distribute themselves like 1D chains between domain boundaries of the sulfur islands as seen in parts c and d of Figure 4.

The amount of the unaffected methylthiolate decreases in an exponential manner with electron exposure as mentioned above, which means that the ESD cross section stays constant independent of the methylthiolate coverage. The ESD process gives rise to several different adsorption states for the methylthiolate as indicated in Figure 4, for example, boundary species located near the periphery of the sulfur islands at low electron exposure and 1D-chain species at high electron exposure. If the cross section varies for such different adsorption states of the methylthiolate, it should depend on the coverage. The coverage-independent cross section indicates that the cross section is invariable for all the different adsorption states of the methylthiolate. Thus, this ESD is considered to occur with the same probability independent of surroundings of the methylthiolate over the surface at any stage of the process. If so, the sulfur adatoms formed by the ESD should exhibit a random distribution at the initial stage of the process, even though they form 2D islands later as shown in the STM images. This is interpreted as facile diffusion and 2D agglomeration of the sulfur adatoms during the ESD process. The facile diffusion of sulfur adatoms on metal surfaces can be inferred from previous findings as formation of several commensurate superstructures depending on the coverage³² and facile 2D-compression by coadsorbed CO.³³ Further, it should be noted that electron-stimulated surface migration of adsorbates has been found for several adsorption systems.^{34,35} There is the possibility that this phenomenon plays an important role in the significant diffusion of the surface species.

Figure 5 shows magnified STM images with molecular resolution for the surface shown in Figure 4c. We observe 1D rows of bright spots along the $\langle 1\bar{2}1 \rangle$ direction and bright bands composed of disordered spots that cross the 1D rows. Both of these structures are associated with the unaffected methylthiolate. The thiolate–thiolate distance along the 1D row is 5.0 Å, which corresponds to the next-nearest-neighbor distance of the

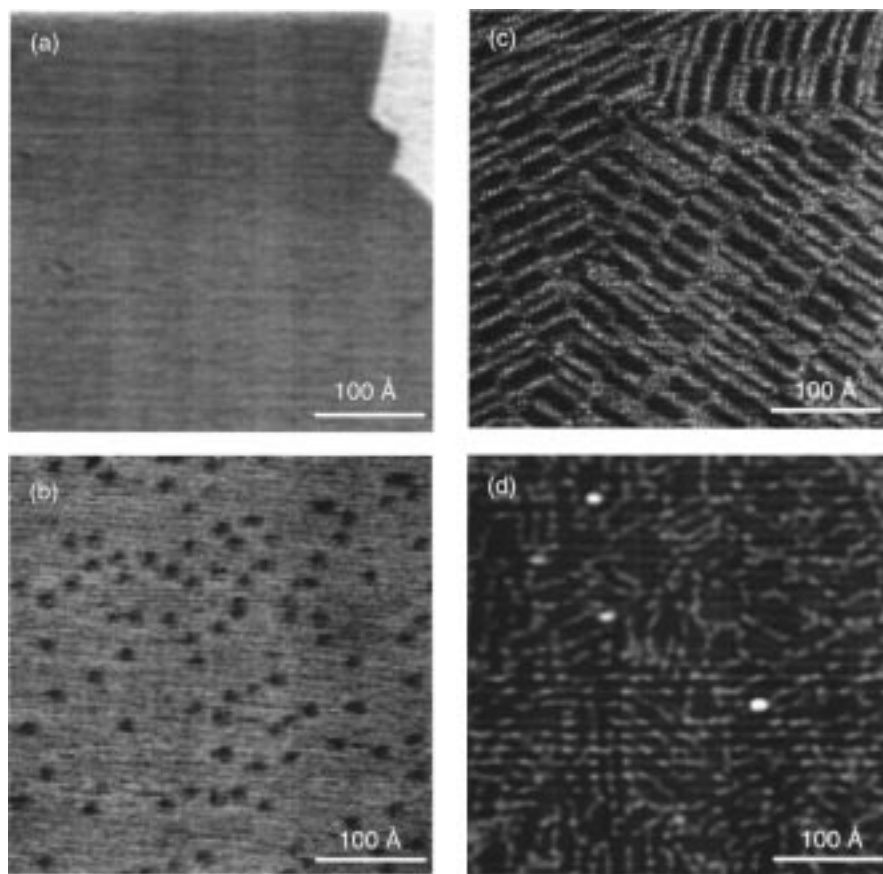


Figure 4. STM images for methylthiolate-covered Au(111) surfaces before (a) and after (b–d) electron irradiation. The electron-beam energy of 4 keV was used. The number of irradiated electrons were (b) 1.6×10^{15} , (c) 7.8×10^{15} , and (d) 3.9×10^{16} electrons/cm².

Au(111) surface atoms (4.99 Å, $\sqrt{3}$ spacing). Therefore, the 1D-chain structure is characterized as a close-packed row of the $(\sqrt{3} \times \sqrt{3})R30^\circ$ commensurate superstructure of Au(111). Interestingly, it is a common tendency for thiols to arrange into a $\sqrt{3}$ chain on Au(111) at submonolayer coverages.^{36,37} The disordered structures across the 1D rows are specifically observed at such places where two different 1D rows come across alternately. In other words, the disordered structure is seen at antiphase domain boundaries of the 1D-chain structure. The fuzzy image for the disordered structure is probably due to site fluctuation of the methylthiolate at the domain boundaries. In fact, positions of the bright spots in the disordered structures change every frame.

To observe the sulfur islands in more detail, we took STM images for surfaces after high electron exposure with low-impedance conditions as shown in Figure 6. Bright but indistinct small clusters in Figure 6a, which interconnect with one another resulting in chain structures, are attributed to the unaffected methylthiolate. Since this surface is at the final stage of the ESD process, the methylthiolate chains are broken at places. Inside regions surrounded by the methylthiolate chains, which should be occupied by the sulfur islands, we can see arrays of rows that are parallel to two of three equivalent $\langle 10\bar{1} \rangle$ directions (A and B). The inter-row spacing is 5.0 Å, which corresponds to the spacing between every second close-packed $\langle 10\bar{1} \rangle$ atomic row of Au(111). Figure 6b shows an STM image for a surface after the ESD process is completely finished. In this image, the methylthiolate chains are no longer observed, while 2D arrays of rows of the sulfur adatoms cover the whole surface. The inter-row periodicity perpendicular to the $\langle 10\bar{1} \rangle$ direction is 5.0 Å. It should be noted that a significant number

of antiphase domain boundaries appear as dark troughs on the surface (indicated by black arrows), resulting in fairly small domain sizes (less than about 100 Å). These domain boundaries might be traces of the methylthiolate chains, which are seen in Figure 6a.

It is interesting to discuss these results from the viewpoint of electron-beam lithography. Gillen et al.¹³ studied the replacement of decanethiol ($\text{CH}_3(\text{CH}_2)_9\text{SH}$) monolayer on silver with fluoromercaptane ($\text{CF}_3(\text{CF}_2)_2(\text{CH}_2)_2\text{SH}$) after electron-beam irradiation once they removed decanethiols in particular areas of the monolayer by electron-beam irradiation and then immersed this sample in a solution of fluoromercaptane. The coverage of the fluoromercaptane on the irradiated areas was only 50% of the full-monolayer coverage. This low efficiency for the exchange adsorption was explained in terms of the influence of deposition of carbonaceous residue on the surface resulting from the interaction of the electron beam with gas-phase hydrocarbons. However, the present study suggests that the low efficiency is not only due to such carbon deposition but also to site blocking by the sulfur adspecies inevitably left behind during the ESD process. This residual sulfur species will block readsorption of an alkylthiolate in the electron-irradiated areas because the sulfur adatom is much more strongly bound to Au(111) than alkylthiolates.³⁸ In reality, we have observed in a preliminary experiment that exposing the electron-irradiated surface to gaseous hexanethiol did not show any evidence for adsorption of hexanethiolate on the surface.³⁹

In the case of thiolate monolayers with longer alkyl chains ($\text{CH}_3(\text{CH}_2)_n\text{S}$; $n \geq 1$), another ESD pathway via C–C bond cleavage is also available. The typical C–C bond energy of alkyl chains is almost 2 times larger than those for the Au–S

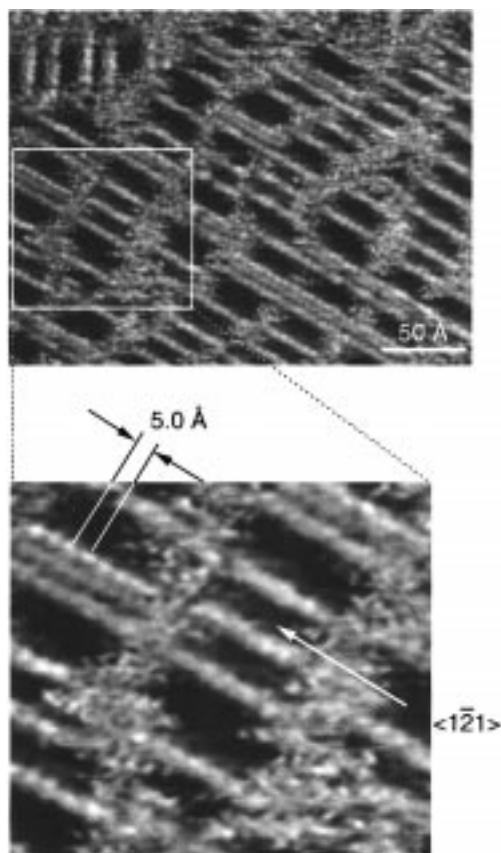


Figure 5. Magnified STM images for an electron-irradiated methylthiolate/Au(111) surface with a medium number of irradiated electrons (7.8×10^{15} electrons/cm²). We observe 1D rows of bright spots along the $\langle 112 \rangle$ direction. The distance between two adjacent bright spots in the row is 5.0 Å. These bright spots are associated with unaffected methylthiolates.

and the S–C bonds at the CH₃S/Au(111) interface.^{38,40} However, since the ESD processes involve electronically excited states induced by electron irradiation, the cross section for each channel cannot be simply related to the bond strength in the ground state. Furthermore, the quenching of such electronically excited states due to the metal substrate is an important factor to the cross section and proximity of the excited bond to the metal surface strongly reduces the cross section.²⁴ Since alkyl chains in most of the thiolate monolayers are aligned in an upright configuration,^{1,23,29} the C–C bonds are less influenced by the quenching compared to the Au–S and S–C bonds. Thus, the contribution of the alkyl-chain cleavage might become significant for longer alkyl-chain thiolates. This causes formation of various thiolates with different alkyl-chain lengths. In any case, to achieve high efficiency for the electron-beam lithographic process, it is necessary to develop an effective method for dissociating the Au–S bond at alkylthiolate/Au interfaces.

Conclusions

We have studied effects of electron irradiation on a methylthiolate monolayer on Au(111) with AES, LEED, TDS, and STM. Electron-beam irradiation on the CH₃S/Au(111) surface induces an ESD of methylthiolate in which mainly the methyl moiety desorbs via S–C bond cleavage leaving a sulfur adatom on the surface. During the ESD process, the sulfur adatoms formed by the ESD exhibit 2D island growth through surface diffusion and agglomeration, while the unaffected methylthiolate species are distributed at domain boundaries of the sulfur islands,

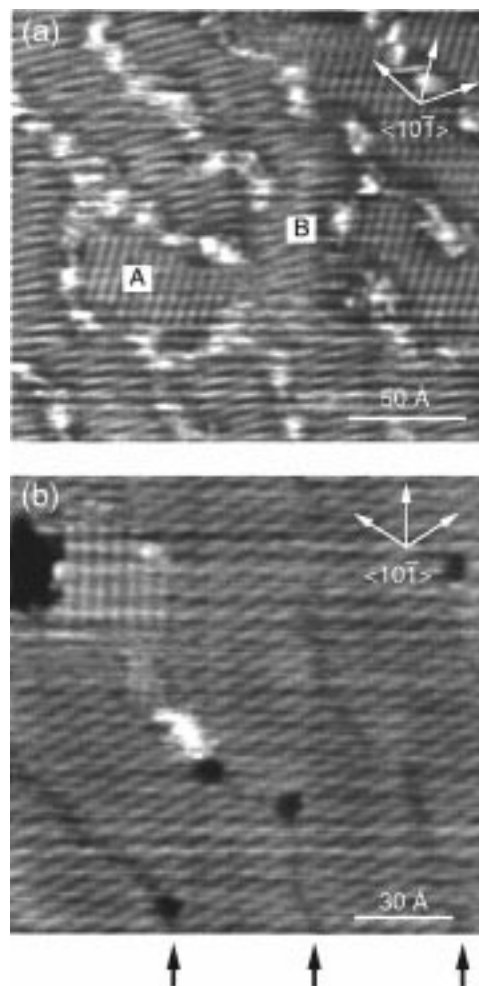


Figure 6. Magnified STM images for highly electron-irradiated methylthiolate/Au(111) surfaces with the number of irradiated electrons of 3.9×10^{16} electrons/cm² (a) and 7.5×10^{17} electrons/cm² (b). These images were taken with lower impedance conditions ((a) 1.0 V and 400 pA; (b) 1.0 V and 210 pA). Bright chains are associated with unaffected methylthiolates, while 2D arrays of rows surrounded by the methylthiolate chains are ascribed to sulfur islands. “A” and “B” marked in Figure 6a indicate two different domains of which the rows are parallel to two $\langle 101 \rangle$ directions. The surface shown in Figure 6b is almost covered with the 2D array of the rows that are attributed to sulfur islands produced from the ESD process. Black arrows in Figure 6b indicate antiphase domain boundaries of the sulfur islands. A bright feature close to the center is not attributed to remaining methylthiolates but to a contamination from a W tip or a Au adcluster, judging from its height.

with forming chain structures. After the completion of the ESD, the Au(111) surface is covered with small patches (≤ 100 Å) of the sulfur islands. These residual sulfur islands act as a suppresser for refilling of an alkylthiolate in the electron-irradiated areas.

References and Notes

- (1) Dubois, L. H.; Nuzzo, R. G. *Annu. Rev. Phys. Chem.* **1992**, *43*, 437.
- (2) Poirier, G. E.; Pylant, E. D. *Science* **1996**, *272*, 1145 and references therein.
- (3) Swalen, J. D.; Allara, D. L.; Andrade, J. D.; Chandross, E. A.; Garoff, S.; Israelachvili, J.; McCarthy, T. J.; Murray, R.; Pease, R. F.; Rabolt, J. F.; Wynne, K. J.; Yu, H. *Langmuir* **1987**, *3*, 932.
- (4) Abott, N. L.; Folkers, J. P.; Whitesides, G. M. *Science* **1992**, *257*, 1380.
- (5) Wollman, E. W.; Frisbie, C. D.; Wrighton, M. S. *Langmuir* **1993**, *9*, 1517.

- (6) Frisbie, C. D.; Wollman, E. W.; Martin, J. R.; Wrighton, M. S. *J. Vac. Sci. Technol.* **1993**, *A11*, 2368.
- (7) Wollman, E. W.; Kang, D.; Frisbie, C. D.; Lorkovic, I. M.; Wrighton, M. S. *J. Am. Chem. Soc.* **1994**, *116*, 4395.
- (8) Tarlov, M. J.; Burgess, D. R. F., Jr.; Gillen, G. *J. Am. Chem. Soc.* **1993**, *115*, 5305.
- (9) Kang, D.; Wrighton, M. S. *Langmuir* **1991**, *7*, 2169.
- (10) Tiberio, R. C.; Craighead, H. G.; Lercel, M.; Lau, T.; Sheen, C. W.; Allara, D. L. *Appl. Phys. Lett.* **1993**, *62*, 1.
- (11) Lercel, M. J.; Tiberio, R. C.; Chapman, P. F.; Craighead, H. G.; Sheen, C. W.; Parikh, A. N.; Allara, D. L. *J. Vac. Sci. Technol.* **1993**, *B11*, 2823.
- (12) Sondag-Huethorst, J. A. M.; van Helleputte, H. R. J.; Fokkink, L. G. *J. Appl. Phys. Lett.* **1994**, *64*, 285.
- (13) Gillen, G.; Wight, S.; Bennett, J.; Tarlov, M. *J. Appl. Phys. Lett.* **1994**, *65*, 534.
- (14) Berggren, K. K.; Bard, A.; Wibur, J. L.; Gillaspay, J. D.; Helg, A. G.; McClelland, J. J.; Rolston, S. L.; Phillips, W. D.; Prentiss, M.; Whitesides, G. M. *Science* **1995**, *269*, 1255.
- (15) Kim, Y.-T.; Bard, A. J. *Langmuir* **1992**, *8*, 1096.
- (16) Ross, C. B.; Sun, L.; Crooks, R. M. *Langmuir* **1993**, *9*, 632.
- (17) Schoer, J. K.; Ross, C. B.; Crooks, R. M.; Corbitt, T. S.; Hampden-Smith, M. J. *Langmuir* **1994**, *10*, 615.
- (18) Kumar, A.; Biebuyck, H. A.; Whitesides, G. M. *Langmuir* **1994**, *10*, 1498.
- (19) Singhvi, R.; Kumar, A.; Lopez, G. P.; Stephanopoulos, G. N.; Wang, D. I.; Whitesides, G. M.; Ingber, D. E. *Science* **1994**, *264*, 696.
- (20) Laibinis, P. E.; Graham, R. L.; Biebuyck, H. A.; Whitesides, G. M. *Science* **1991**, *254*, 981.
- (21) Graham, R. L.; Bain, C. D.; Biebuyck, H. A.; Laibinis, P. E.; Whitesides, G. M. *J. Phys. Chem.* **1993**, *97*, 9456.
- (22) Nuzzo, R. G.; Zegarski, B. R.; Dubois, L. H. *J. Am. Chem. Soc.* **1987**, *109*, 733.
- (23) Dubois, L. H.; Zegarski, B. R.; Nuzzo, R. G. *J. Chem. Phys.* **1993**, *98*, 678.
- (24) Basu, P.; Chen, J. G.; Ng, L.; Colaianni, M. L.; Yates, J. T., Jr. *J. Chem. Phys.* **1988**, *89*, 2406.
- (25) Whitten, J. E.; Young, C. E.; Pellin, M. J.; Gruen, D. M.; Jones, P. L. *Surf. Sci.* **1987**, *184*, L332.
- (26) Widrig, C. A.; Alves, C. A.; Porter, M. D. *J. Am. Chem. Soc.* **1991**, *113*, 2805.
- (27) Alves, C. A.; Smith, E. L.; Porter, M. D. *J. Am. Chem. Soc.* **1992**, *114*, 1222.
- (28) Poirier, G. E.; Tarlov, M. *J. Langmuir* **1994**, *10*, 2853.
- (29) Fenter, P.; Eberhardt, A.; Liang, K. S.; Eisenberger, P. *J. Chem. Phys.* **1997**, *106*, 1600.
- (30) Kondoh, H.; Nozoye, H. To be published.
- (31) We could observe molecular images for CH₃CH₂S/Au(111) at room temperature.
- (32) For example, see the following. Kostelitz, M.; Domanfe, J. L.; Oudar, J. *Surf. Sci.* **1973**, *34*, 431. Berthier, Y.; Perdureau, M.; Oudar, J. *Surf. Sci.* **1973**, *36*, 225.
- (33) McIntyre, B. J.; Salmeron, M.; Somorjai, G. A. *Surf. Sci.* **1995**, *323*, 189.
- (34) Fedorus, A. G.; Gonchar, V. V.; Kanash, O. V.; Klimenko, E. V.; Naumovets, A. G.; Zaslomovich, I. N. *Surf. Sci.* **1991**, *251/252*, 846.
- (35) Jansch, H. J.; Xu, J.; Yates, J. T. J., Jr. *J. Chem. Phys.* **1993**, *99*, 721.
- (36) Poirier, G. E.; Tarlov, M. J.; Rushmeier, H. E. *Langmuir* **1994**, *10*, 3383.
- (37) Camillone, N., III; Leung, T. Y. B.; Schwartz, P.; Eisenberger, P.; Scoles, G. *Langmuir* **1996**, *12*, 2737.
- (38) Sellers, H. *Surf. Sci.* **1993**, *294*, 99.
- (39) The electron-irradiated surface was exposed to 400 langmuirs of gaseous hexanethiol (C₆H₁₃SH) at room temperature. Although such exposure of hexanethiol to clean Au(111) gives rise to complete covering of Au(111) with a "striped phase" (see refs 36 and 37), no hexanethiol-induced structure was observed in the STM image after the exposure.
- (40) The Chemical Society of Japan, Eds. *Kagaku-Binran*, 3rd ed.; Maruzen: Tokyo, 1984; Chapter 9.